ELSEVIER

Contents lists available at ScienceDirect

Precision Engineering

journal homepage: www.elsevier.com/locate/precision





Line-edge-roughness characterization of photomask patterns and lithography-printed patterns

Zhikun Wang ^a, Pengfei Lin ^a, Phuc Nguyen ^a, Jingyan Wang ^a, ChaBum Lee ^{a,*}

^a J. Mike Walker '66 Department of Mechanical Engineering, Texas A&M University, 3123 TAMU, College Station, TX 77843-3123, USA

ARTICLE INFO

Handling Editor: Prof. R. Leach

Keywords: Lithography Photomask Line-edge-roughness (LER) Fringe analysis Metrology and inspection

ABSTRACT

This paper presents the line-edge-roughness (LER) characterization of the photomask patterns and the lithography-printed patterns by enhanced knife edge interferometry (EKEI) that measures the interferometric fringe patterns occurring when the light is incident on the patterned edge. The LER is defined as a geometric deviation of a feature edge from an ideal sharp edge. The Fresnel number-based computational model was developed to simulate the fringe patterns according to the LER conditions. Based on the computational model, the photomask patterns containing LER features were designed and fabricated. Also, the patterns were printed on the glass wafer by photolithography. The interferometric fringe patterns of those two groups of patterns were measured and compared with the simulation results. By using the cross-correlation method, the LER effects on the fringe patterns were characterized. The simulation and experimental results showed good agreement. It showed that the amplitude of the fringe pattern decreases as the LER increases in both cases: photomask patterns and printed wafer patterns. As a result, the EKEI and its analysis methods showed the potential to be used in photomask design and pattern metrology, and inspection for advancing semiconductor manufacturing processes.

1. Introduction

Lithography as one of the key semiconductor manufacturing processes writes the projected patterns on the wafer substrate from the photomask pattern image, and the exposure light wavelength and numerical aperture (NA) of the lens system are critical to determining the lithography printing resolution [1-3]. Many chip makers thrive to achieve large-volume yield and high performance, printing small linewidth or feature width, the so-called critical dimension (CD), in their mass production. In lithography, chip makers can achieve smaller CD by using shorter light wavelength and larger NA based on the Rayleigh criterion [3]. It is because the shorter light wavelength light lowers the diffraction effect. In a recent lithography technology, deep ultraviolet lithography (DUVL) uses an excimer laser source that produces either 193 or 248 nm wavelength, and extreme ultraviolet lithography (EUVL) uses a 13.5 nm wavelength light (high power laser to create a plasma) to transfer the patterns from the reflective photomask to the wafer substrate [4]. EUVL was recently adopted for high-volume chip manufacturing along with EUV photomask and photoresist development in 2019, being capable of 125 wafer throughput per hour [5].

Rayleigh criterion determines printing resolution in lithography, so

chip manufacturers are eager to use the smaller wavelength light and high NA optical systems. It is always true when the photomask is defect free. Metrology and inspection for photomask manufacturing and quality management minimize the potential printing error, enhance yield, and reduce the scraps [6,7]. In the lithography process, the defects such as dust, particles, scratches, or residual resins on the photomask can lower pattern printability. Besides such defects, the line-edge-roughness (LER) negatively impacts CD variation in lithography printing processes [8]. The photomask inspection and printability test methods have been widely studied for a few decades ago. The most common methods are based on atomic force microscopy (AFM), scanning electron microscopy (SEM), transmission electron microscopy (TEM), or X-ray scatterometry [9-14]. AFM uses a small and pointy tip for nanometer-level scanning or indentation and provides high axial and lateral resolution, and SEM and TEM use a finely focused electron beam to image the target surface. While these methods facilitate the visualization of high-resolution images of various defects, each presents specific limitations. AFM is hindered by a relative slow scanning speed; SEM demands an environment of high vacuum environment for optimal operation; TEM is only suitable for very thin sample and requires complex sample preparation; X-ray Scatterometry, while non-destructive,

E-mail address: cblee@tamu.edu (C. Lee).

^{*} Corresponding author.

Z. Wang et al. Precision Engineering 88 (2024) 235–240

offers relatively lower resolution and demands complex data interpretation. Therefore, chip manufactures have been continuously seeking advanced methods for online measurement, inspection, and artificial intelligence-based analysis. Recently, several companies have developed new inspection systems; however, these systems are immature and expensive, and there are technological gaps that need to be addressed before the new technology can be adopted in semiconductor manufacturing processes.

The authors introduced knife-edge interferometry (KEI) which measures the interferometric fringe patterns occurring when the light is incident on the sharp edge. This method was further improved by focusing the beam, the so-called enhanced knife-edge interferometry (EKEI) that creates the spherical wavefront at the front of the edge and produces higher spatial frequency fringes from the various edges such as cutting tools, razor blades, and photomask width and linewidth [15–19]. Here EKEI was employed to characterize the LER in both photomask and the lift-off printed wafer by lithography, and the LER effects on the KEI fringe patterns were characterized. Also, the LER effect on the EKEI was simulated by the Fresnel number-based computational model, and the computational and experimental results were compared. Also, the data analysis method based on cross-correlation was discussed.

2. Methods and simulations

In this study, the simulation model was developed by using the Fresnel number-based geometry optic model. In addition, the LER was characterized in the simulation model for comparison. Fig. 1 shows the schematic of the EKEI-based measurement principle. The proposed measurement system comprises a laser diode, an aperture, an objective lens, a photodetector (PD) sensor, and a 2-degree-of-freedom XY scanning stage. The objective lens creates spherical waveforms by shaping the incident collimated light. The PD sensor collects the interferometric fringe patterns induced by edge diffraction while scanning the photomask. The details of the principle of the EKEI system can be referred to the author's previous study [15]. In the EKEI system, the objective lens-generated spherical waveform will form a Fresnel zone on the photomask surface, which is directly related to the Fresnel number of the optical system. The equation of the Fresnel number can be found in Eq. (1). The odd term of the Fresnel zone implies the constructive contribution to the interference while the even number of the Fresnel zone means the destructive contribution to the interference.

$$F = \frac{\alpha^2}{\lambda \times Z_{eff}}.$$
 (1)

In this equation, α is the radius of the beam at the photomask plane, λ is the light wavelength, Z_{eff} is the effective distance of the optical system. Equation (1) can be simplified as [15],

$$F = \frac{NA^2 \times Z_{src}}{\lambda}.$$
 (2)

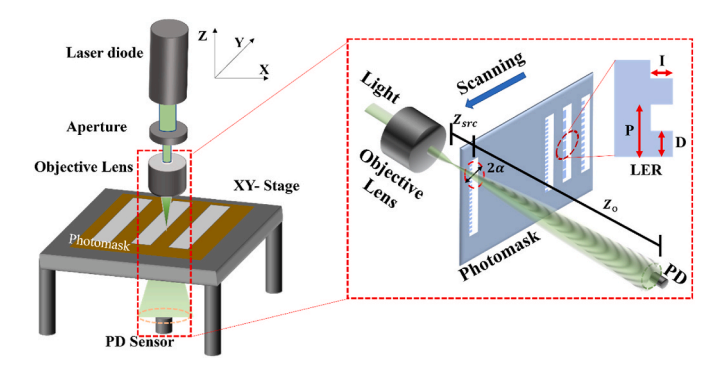


Fig. 1. Measurement method: Enhanced knife-edge interferometry.

where, NA is the numerical aperture of the objective lens, $Z_{\rm src}$ is the distance between the objective lens focal point and the photomask pattern layer along the Z axis. The EKEI-based measurement system parameter and LER parameter was included in the simulation model. In the simulation model, the LER parameter was defined as three times the standard deviation (σ) of the edge profile as [20].

$$LER = 3 \times \sigma. \tag{3}$$

In the simulation, the LER was defined by a periodic rectangular function with a different duty cycle (D/P) and intensity (I). Here, D and P indicate the depth and period of the LER. The schematic of these two parameters was depicted in Fig. 1. Therefore, the LER can be expressed by duty cycle and intensity as,

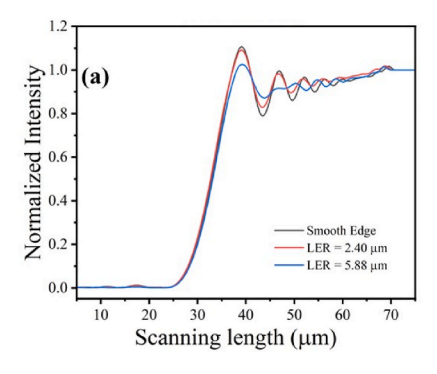
$$LER = 3 \times I\sqrt{\frac{D}{P} \times \left(1 - \frac{D}{P}\right)}.$$
 (4)

By blocking different amounts of Fresnel zone, the PD sensor can capture the interferometric fringes. In that case, the edge geometric profile can affect the amount of blocking area in the Fresnel zone, thus, the LER can be traced by referring to the changes in fringe patterns. The 9 groups of various LER conditions were simulated and analyzed in the developed simulation model. Fig. 2 shows the changes in fringe patterns regarding 3 different LER parameters. In the results of simulated fringe patterns, by adding different amounts of LER value into the model, the fringe of assigned datasets will attenuate based on the extent of edge roughness. As the LER value increases, all simulation datasets find a strong attenuation in the first and second order of fringes. When the LER value increases to 2.40 μ m and 5.88 μ m, the amplitude for the first order fringes decreases by 2% and 9%, respectively.

The generated fringe pattern was analyzed by using the crosscorrelation-based analysis method [15]. In these 10 datasets of the simulated fringes, there are 9 simulated experiment groups and 1 simulated control group with a smooth edge. The LER was defined by periodic rectangular functions with different intensities and duty cycle, the duty cycle varies from 0.2 to 0.4 with an interval equal to 0.1, and the intensity changes from 2 μm to 4 μm with a 1 μm interval. Based on the designed periodic rectangular function and Eq. (4), the LER value changes from 2.40 μm to 5.88 μm . The cross-correlation method aims to feature the difference between each group by analyzing the similarity value of the interferometric fringe pattern of each case regarding the reference group. By setting group 10 (smooth) as a reference group, the similarity value from experiment groups drops from 0.997 (LER equals $2.40~\mu m)$ to 0.965 (LER equals $5.88~\mu m$). From the result based on the simulated fringe pattern in Fig. 2(b), the similarity decreases when LER increases.

3. Experiments

Fig. 3 describes the experimental setup. A collimated (λ 532 nm) laser passes through a φ 1.0 mm aperture and is beam-shaped by an objective lens (NA 0.4). The beam-shaped laser will pass through the photomask, and then, the diffraction fringe pattern can be recorded by the PD sensor. The beam diameter on the photomask surface is about 100 μm in the current setup. A photomask with 9 groups of line patterns containing different characterized LER was tested during the experiment. The photomask was securely fixed on an XY motorized scanning stage, and the scanning speed was set to 1 mm/s. By scanning different areas on the photomask, the fringe patterns created from different LER decorated lines can be recorded. The signal was recorded by an optical fiber-pigtailed photodiode and a lock-in amplifier was used for signal processing. While all datasets from the photomask were recorded, the photomask was used for lithography to make a lift-off replica wafer with the Cr coating layer. After the lithography process, both the photomask and the replica wafer patterns were measured by optical microscopy.



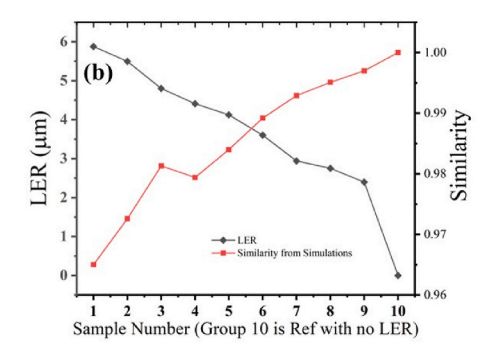


Fig. 2. (a) Simulated fringe pattern with different LER conditions, (b) similarity for different LER condition-generated fringe pattern based on cross-correlation method.

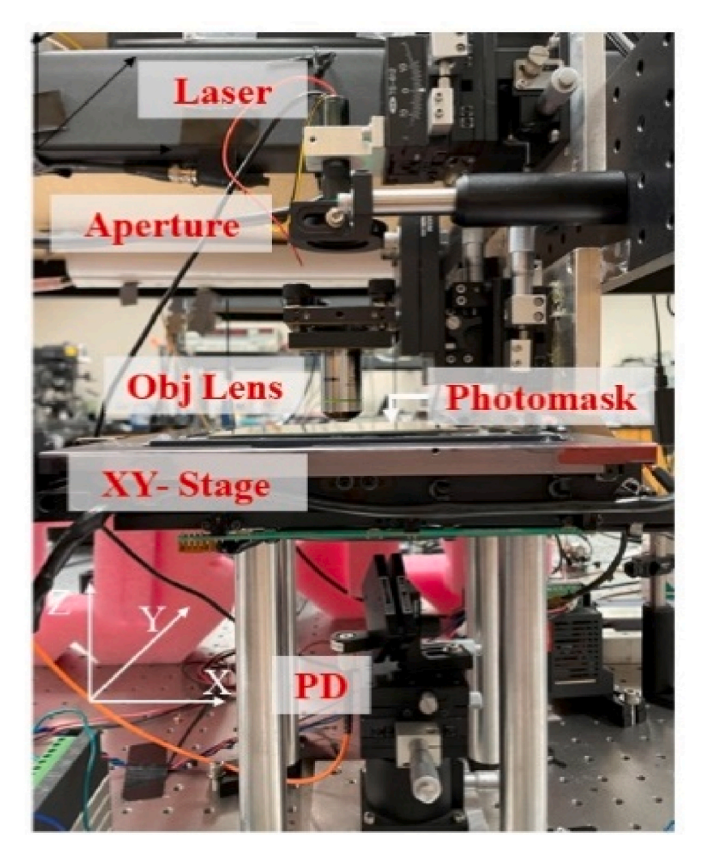


Fig. 3. Experiment setup.

The LER values from the design, photomask, and printed wafer patterns are shown in Fig. 4. Fig. 5 shows the picture of those patterns from the design, photomask, and its replica wafer from lift-off lithography. The LER values for the photomask and wafer in Fig. 4 were calculated by analyzing the microscopic images. From Fig. 4, in general, the LER value decreases with group number increases in both photomask and replica wafers. However, there are still some differences between the real product and the design. First, although the photomask product keeps the designed LER pattern from Fig. 5, there is still about a 1 μ m LER deviation compared with the design and photomask LER, which may be caused by the resolution of the image. In those images, $10 \mu m$ implies 34-pixel points. In that circumstance, it is hard to define the position of the edge precisely due to the diffraction when taking the pictures. A 1 μm of LER deviation shows a 0.33 μm difference in standard deviation, which is just a 1-pixel variance, which might be the reason for the LER deviation between the design and real photomask. There are also deviations between the photomask LER and the wafer LER. For that issue,

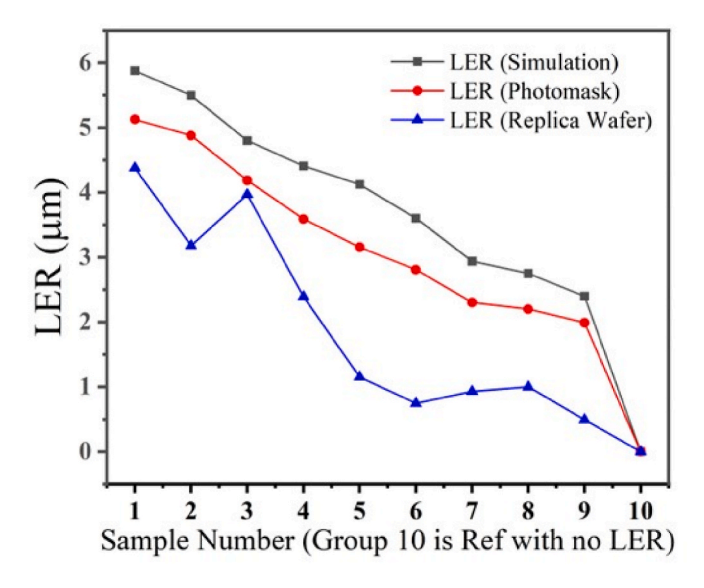


Fig. 4. LER values calculated from design, photomask, and printed wafer patterns.

one of the reasons might be the resolution of the picture, and the others may be caused by the lithography process. The replica wafer was fabricated by lift-off processing [21]. During the manufacturing process, there were many uncertainties that might have caused imperfection in duplication because of diffraction, scattering, photoresist, or catalyst during the lithography. Last, the replica wafer was scanned by the EKEI system to record the fringe patterns in comparison with those of the photomask patterns.

In the real industrial applications, LER patterns are typically more irregular and complex than simple periodic rectangular functions due to influences from multiple factors like lithography, etching processes, and material properties. Despite this complexity, the method can still offer valuable insights into fundamental behaviors and impacts of LER, such as changes in fringe intensity and internal distance, and can help estimate actual LER in real-world applications.

4. Results

The EKEI system scanned the photomask and its replica wafer. As mentioned in the simulation section, on the photomask, there are 9-line patterns with different LER values, and the LER was defined by the intensity and duty cycle for the rectangular function on the edge. From group 1 to group 9, The LER value decreases from 5.88 μ m to 2.40 μ m. Group 10 was designed as a control group with no LER (smooth edge) for comparison. Fig. 6 shows the fringes recorded from the photomask and wafer under different LER conditions (smooth condition, LER 2.40 μ m,

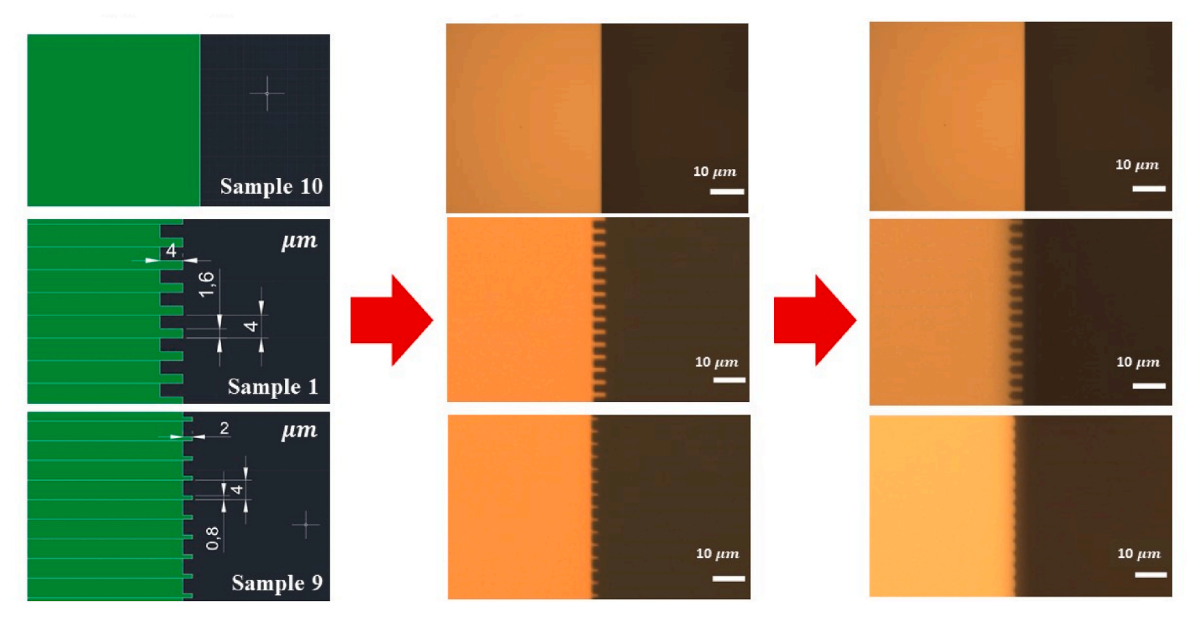


Fig. 5. Photomask LER design and images of the fabricated patterns: (a) photomask LER design (left), (b) images of real photomask with designed LER (middle), and (c) images of replica wafer with LER (right).

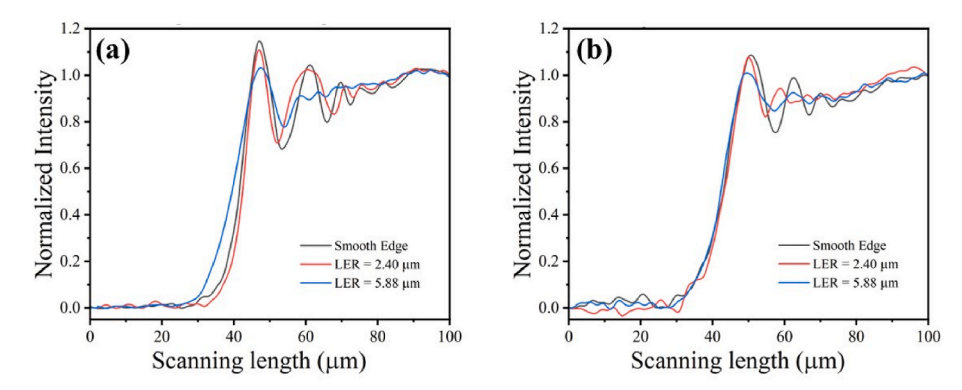


Fig. 6. Interferometric fringe patterns: (a) photomask pattern and (b) wafer patterns.

and 5.88 μm). The 2.40 μm LER and 5.88 μm LER implies the lowest and the highest LER value in this study.

Based on the fringes from Fig. 6(a), the fringes get attenuated when the LER value increases. When the LER changes from smooth (LER =0) to LER $=5.88~\mu m$, the intensity of the first order fringe decreases from 1.147 to 1.028. Not only does the amplitude of the first-order fringe decrease, but the higher-order fringes also get attenuated or vanished when the LER value increases. In Fig. 6(a), compared with the 5 orders of fringes from the smooth case, when the LER increases to 5.88 μm , only the first and the second order of fringes can be distinguished, and all higher order fringes get vanished. Fig. 6(b) shows the scanning result from the replica wafer. Comparing Fig. 6(a) and (b), the fringes generated by the replica wafer keep the trend of attenuation as same as the fringes from the photomask. The trend of the fringe pattern showed good agreement with the simulation results in Fig. 4. Overall, the experimental approaches showed the following results:

- 1. The LER can be printed on the photomask and can be replicated to the wafer by photolithography.
- 2. The fringes from edge diffraction get attenuated when the LER value of the edge increases. The similarity decreases by 0.017 when the LER value changes from 2.40 μm to 5.88 μm . Because of the attenuation, the intensity for the first-order fringe will decrease and some higher-order fringes will vanish.

After collecting the fringe patterns from the photomask edge patterns under different LER conditions, the cross-correlation-based similarity value can numerically express the features that represent a change in the fringes. This method was first proposed in the previous research [18] for edge roughness characterization, and the value is calculated by dividing the covariance of two signals with their respective standard deviation as:

$$SI = \frac{\sum_{i=1}^{n} (X_i - \overline{X})(Y_i - \overline{Y})}{\sqrt{\sum_{i=1}^{n} (X_i - \overline{X})^2} \sqrt{\sum_{i=1}^{n} (Y_i - \overline{Y})^2}}$$
(5)

Here X and \overline{X} are the reference fringe pattern and its mean value, while Y and \overline{Y} are the fringes of LER edge and its mean value, respectively. Total number of datasets is noted as n, and i indicates an i-th data order. When two fringes are identical, the cross-correlation becomes 1. The analysis results from the cross-correlation method can be found in Fig. 7. This result showed that the similarity increases while the LER decreases. Based on the similarity results from photomask fringe patterns, the similarity decreases by 0.0183 when the LER value changes from 2.40 μ m to 5.88 μ m. Although the basic dimension of the characterized rectangular function follows the LER pattern design (intensity and duty cycle), there are still some deviations from the design drawing and actual photomask features, which causes the difference in the variation of similarities. Plus, the diffraction and the imperfection of the lift-off replica wafer induce the error between the replica wafer and the

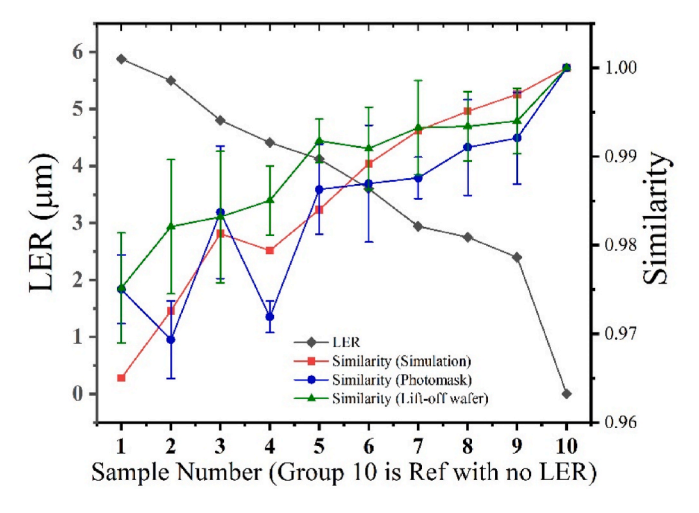


Fig. 7. LER characterization: result by cross-correlation method.

photomask, which causes the deviation of the similarity values as well. But these results show that the EKEI system can track and characterize the LER based on the changes in similarity values. The similarity has a negative correlation with the LER value.

Fig. 8 shows the fringe pattern changes in case there is a residue on the photomask after the lithography process. Compared with the fringes from the smooth edge, the fringe from an abnormal (residue-contaminated) edge shows different features. First, the boundary of the edge becomes fuzzy. In a conventional coated pattern, the light intensity increases dramatically when the incident light is not blocked by the opaque pattern, which follows the trend in Fig. 8, normal edge, from 100 μm to 200 µm. However, the boundary for a residue-contaminated pattern does not follow that feature. In Fig. 8, the abnormal edge plot, from 100 μm to 250 μm, shows that the normalized intensity increases gradually. The abnormal edge did not block the light 100 percent, the light can partially pass through the edge and its contaminated area. Second, the fringe pattern vanished in fringes from the abnormal edge. It may cause by the difference in the light interference. Based on the Huygens-wavelet theory [16], the incoming light source and the Huygens wavelets emitted on the edge generates the edge diffraction pattern. However, when the edge changes to an abnormal edge, not only do we have the incoming light source and Huygens wavelets from the edge, but we also have the light that is modulated by that residue-contaminated area. This third wave source can change the fringe pattern from the conventional edge diffraction. Based on the results from Fig. 8, the EKEI system can also track the variance of the fringes when the residue photoresist damages or contaminated the photomask. In that case, the EKEI system may be effective for an in-situ photomask monitoring system to track the status of the photomask in industries. The EKEI system can track and report those residues directly in the semiconductor manufacturing process.

5. Conclusion and future works

This paper showed the EKEI-based system for LER characterization. The Fresnel number-based geometrical EKEI model with LER characterization was developed. The EKEI model could simulate interferometric fringe patterns concerning different LER conditions. The LER of the pattern was characterized by using rectangular functions in different duty cycles and intensities. The simulation results showed that the increase in the LER value result in attenuation of the fringe pattern. In addition, the cross-correlation method analyzed the generated fringe pattern. As a result, the similarity value decreased as the LER increased. It also implemented this analytical method in experimental data analysis. From the experiment, LER-characterized photomask patterns and lithography-printed patterns recorded the fringes. The computation

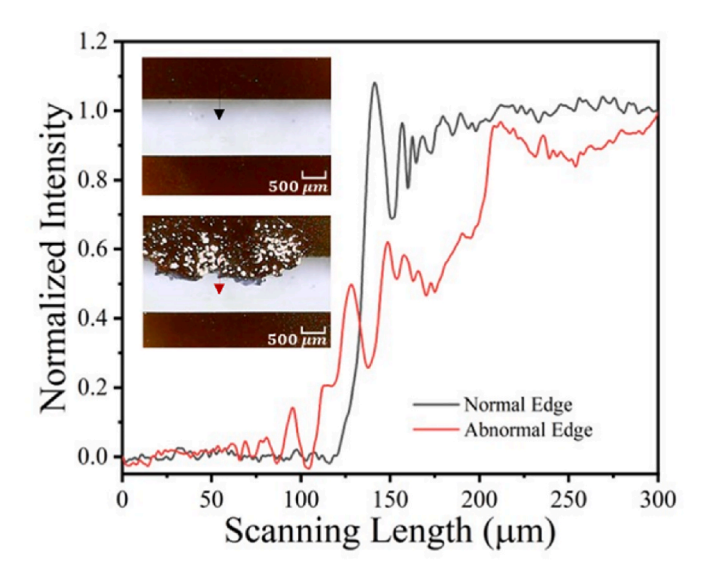


Fig. 8. Comparison in interferometric fringe patterns between a smooth (normal) edge and residue-contaminated (abnormal) edge.

model shows great agreement with the experimental results obtained from the cross-correlation analysis method. As a result, EKEI can characterize the LER on both the photomask patterns and the printed patterns. Successful integration of the proposed inspection system sheds light not only on the LER characterization but also on photomask defectivity metrology and inspection, improving the lithography processes and increasing yield.

Author's contribution

All authors contributed equally to this work.

Data availability

The data that supports the findings of this study are available from the corresponding author upon reasonable request.

Declaration of competing interest

The authors declare that they have no known competing financial interests or personal relationships that could have appeared to influence the work reported in this paper.

Acknowledgment

This research has been supported by National Science Foundation (CMMI #1855473, #212499). We also appreciate AggieFab at Texas A&M University for fabrication process discussion and data acquisition.

References

- Yoshioka N, Terasawa T. Advanced mask inspection and metrology. In: AIP conference proceedings, vol. 683. American Institute of Physics; 2003, September. p. 389–95. No. 1.
- [2] Seisyan RP. Nanolithography in microelectronics: a review. Tech Phys 2011;56(8): 1061–73.
- [3] Wood O. EUV lithography: new metrology challenges. In: AIP conference proceedings, vol. 931. American Institute of Physics; 2007, September. p. 375–81. No. 1.
- [4] French RH, Gordon JS, Jones DJ, Lemon MF, Wheland RC, Zhang X, Qiu W. Materials design and development of fluoropolymers for use as pellicles in 157-nm photolithography. Optical Microlithography XIV 2001, September;4346:89–97. SPIE.
- [5] Watanabe T. Current status and prospect for EUV lithography. In: 2017 7th international conference on integrated circuits, design, and verification (ICDV). IEEE; 2017, October. p. 2–7.

- [6] Cross A, Sah K, Anantha V, Gupta B, Ynzunza R, Troy N, Leray P. High sensitivity repeater detection with broadband plasma optical wafer inspection for mask defect qualification. Extreme Ultraviolet Lithography 2020 2020, October;11517:53–60.
- [7] Pang L, Peng D, Hu P, Chen D, He L, Li Y, Tolani V. Computational metrology and inspection (CMI) in mask inspection, metrology, review, and repair. Adv Opt Technol 2012;1(4):299–321.
- [8] Shang E, Zhao H, Li J, An X, Wu T. OffRoadScene: an open database for unstructured road detection algorithms. In: 2013 international conference on computer sciences and applications. IEEE; 2013, December. p. 779–83.
- [9] Goldstein M, Naulleau P. Actinic microscope for extreme ultraviolet lithography photomask inspection and review. Opt Express 2012;20(14):15752–68.
- [10] Keyvani A, Tamer MS, van Es MH, Sadeghian H. Simultaneous AFM nano-patterning and imaging for photomask repair. Metrology, Inspection, and Process Control for Microlithography XXX 2016, March;9778:423–9. SPIE.
- [11] Zandiatashbar A, Kim B, Yoo YK, Lee K, Jo A, Lee JS, Park SI. Automatic defect review for EUV photomask reticles by atomic force microscope. 2015 Photomask Technology 2015, October;9635:302–10. SPIE.
- [12] Holz M, Reuter C, Reum A, Ahmad A, Hofmann M, Ivanov T, Mechold S, Rangelow IW. Atomic force microscope integrated into a scanning electron microscope for fabrication and metrology at the nanometer scale. 2019 Photomask Technology 2019, September;11148:288–95. SPIE.

- [13] Dai G, Hahm K, Sebastian L, Heidelmann M. Comparison of EUV photomask metrology between CD-AFM and TEM. Nanomanufacturing and Metrology 2022: 1–10.
- [14] Orji NG, Badaroglu M, Barnes BM, Beitia C, Bunday BD, Celano U, Kline RJ, Neisser M, Obeng Y, Vladar AE. Metrology for the next generation of semiconductor devices. Nat Electron 2018;1(10):532–47.
- [15] Wang Z, Lin P, Lee C. Preliminary study of photomask pattern inspection by beamshaped knife-edge interferometry. Precision Engineering; 2022.
- [16] Wang Z, Lee C. Knife-edge interferogram analysis for corrosive wear propagation at sharp edges. Appl Opt 2021;60(5):1373–9.
- [17] Wang Z, Chun H, Lee C. Enhancement of knife-edge interferometry for edge topography characterization. Rev Sci Instrum 2021;92(12):125101.
- [18] Jeon S, Stepanick CK, Zolfaghari AA, Lee C. Knife-edge interferometry for cutting tool wear monitoring. Precis Eng 2017;50:354–60.
- [19] Jeon S, Zolfaghari A, Lee C. Dicing wheel wear monitoring technique utilizing edge diffraction effect. Measurement 2018;121:139–43.
- [20] Bonam R, Liu CC, Breton M, Sieg S, Seshadri I, Saulnier N, Shearer J, Muthinti R, Patlolla R, Huang H. Comprehensive analysis of line-edge and line-width roughness for EUV lithography. Extreme Ultraviolet (EUV) Lithography VIII 2017, March; 10143:266–77. SPIE.
- [21] Liao WS, Cheunkar S, Cao HH, Bednar HR, Weiss PS, Andrews AM. Subtractive patterning via chemical lift-off lithography. Science 2012;337(6101):1517–21.